

Soot formation during polyurethane (PU) plastic pyrolysis: the effects of temperature and volatile residence time

Xuebin Wang ^{a,*}, Qiming Jin ^a, Jiaye Zhang ^a, Yan Li ^a, Shuaishuai Li ^a, Hrvoje Mikulčić ^b, Milan Vujanović ^b,

Houzhang Tan ^{a,*}, Neven Duić ^b

^a MOE Key Laboratory of Thermo-Fluid Science and Engineering, Xi'an Jiaotong University, Xi'an, Shaanxi, 710049, China

^b Faculty of Mechanical Engineering and Naval Architecture, University of Zagreb, 10000 Zagreb, Croatia

*Corresponding Author Email: wxb005@mail.xjtu.edu.cn

ABSTRACT

Soot is an undesired co-product during thermal-chemical disposal (incineration, pyrolysis, etc.) of plastic wastes at high temperatures, while also regarded as a valuable nanoscale carbon-based material if with proper production and post-treatment methods. In this paper, the pyrolysis of polyurethane (PU) plastics, a major composition of plastic waste, was conducted in a fixed-bed reactor to investigate the soot formation mechanism in depth. The effects of pyrolysis temperature (1000-1300 °C) and volatile residence time (0.2-2 s) on the yield, micro-morphology, composition and reactivity of soot were studied. Results show that the initialization and growth of soot particles during PU pyrolysis requires a certain high temperature and long volatile residence time. With a volatile residence time of 2 s, the soot yield is 11.0 wt.% at 1000 °C and increases to 24.5 wt.% with the pyrolysis temperature increasing to 1300 °C; while when the volatile residence time decreases to 0.2 s, the soot cannot be observed until 1200 °C. When the pyrolysis temperature increases 1000 °C to 1100 °C, the X-ray diffraction (XRD) patterns indicates an enhanced graphitization thereby a lower reactivity of soot oxidation, which is approved by onion-like layered structures initially observed by the high-resolution transmission electron microscope (HR-TEM) at 1100 °C and 2 s. When the pyrolysis temperature increases from 1100 °C to 1200-1300 °C, NaCl is observed in soot particles, which catalysis promotes the reactivity of soot oxidation. Gas chromatography and mass spectrometer (GC-MS) was used to measure the gas and tar compositions, especially the polycyclic aromatic hydrocarbons (PAHs), are proved essential for the formation of soot precursor. A large number of PAHs with ring number ≥ 4 start to form at 1100-1200 °C. Based on the soot characterization and gas-tar compositions, a pathway from light fragments and mono-ring aromatics to heavier aromatic compounds is proposed aiming to explain the chemical evolution of soot precursor particles.

Keywords: Polyurethane; pyrolysis; soot; volatile residence time; high temperature.

1. Introduction

Providing a fundamental contribution to various modern daily activities, plastics have become essential materials in agriculture, automobile industry, electricity and electronics, construction industry and so on [1]. Among them is polyurethane (PU) plastic, which is an important kind of copolymer containing blocks of polyesters or polyethers of low molecular weight covalently bonded by a urethane group ($-\text{NHCO}-\text{O}-$), widely used in the manufacture of car paints, flexible foams for bedding, rigid foams for insulation, adhesives and other commercial goods [2], and its production has reached 16 million tons per year since 2015. The production of polyurethane plastics of large quantity among which only a small amount is recycled, the majority being not biodegradable, however, leads to an increasing generation of waste. A prevalent way to dispose of wasted PU plastic is landfilling, which induces severe air, water, and soil pollutions [3]. While incineration is normally connected to waste-to-energy management and once considered economical and of high energy recovery rate [4], it is now questioned due to its emission of smoke (particulate matter), particulate-bound heavy metals and volatile organic compounds [5]. Therefore, the adoption of more efficient and environmental-friendly methods is highly urged.

Upgrading of plastic waste through pyrolysis is regarded as one of the most environmental and sustainable treatment methods, since neither will the unbiodegradable deposition be remained nor will the organic compounds in the feedstock be wasted. Being in an inert atmosphere (free from oxygen), pyrolysis succeeds in realizing high efficiency of energy conversion and low emission properties, surpassing the combustion/incineration or gasification methods due to the high energy recover rate, avoided forming pollutant and reduced carbon footprints [6]. In pyrolysis, the thermal cracking processes of polymeric materials under high temperatures lead to the breakdown of macromolecular structures and the formation of a wide range of hydrocarbons. When under modest temperature conditions, three fractions composing of a gas fraction, a liquid fraction, i.e. tar, mainly consisting of paraffins, olefins, naphthenes and aromatics, and a solid residue, i.e. char, are divided from the pyrolytic products. Plenty of studies have reported the investigations on these valuable products including upgraded bio-oil as high quality liquid fuels [7, 8], syngas with high heating value [9, 10] and char for agricultural and catalytic use [11]. To sum up, the distribution of products and their properties from plastic pyrolysis are highly dominated by a series of factors including temperature, pressure, residence time, reactor time and feedstock, etc. [12].

While gas/tar/char products of plastic pyrolysis being extensively studied, another product, soot, which occurs only when pyrolysis temperature is elevated highly enough [13], is raising wide attention. Soot is a highly carbonized, solid-phase compound with a particle size scale of nanometer, in which the carbon mole fraction is over 0.85 [14]. Due to its small particle size, high diffusivity and strong sorption capacity of heavy metals and toxic larger polycyclic aromatic

hydrocarbons (PAHs), soot has become a severe threaten to atmospheric environment and human health, thus a major concern in pollutant emission control. Sufficient studies have confirmed the close relationship between soot formation and pyrolysis volatiles which is mainly dominated by two mechanisms, that is, the hydrogen abstraction/carbon addition (HACA) mechanism [15] and a “ring-ring condensation” interaction [16]. Further surface growth, coalescence and agglomeration lead to the final appearance of soot particles whose diameters are about 20-200 nm, in terms of chains, clusters, dendrites, rings, spheroids, flakes and other types [17]. Physical and chemical characteristics of soot particles, such as the inception particle size, structure of the aggregates and soot reactivity, highly depend on the types of fuels whose varied chemical compositions lead to totally different reaction pathway, and reaction conditions which determine the circumstances the soot particles originate. For instance, a wide variation of temperature allows a shift of soot particle size distribution to be observed [18], while under higher pressure the particles were compressed to form small smooth pellets [17]. Soot yields and morphologies also showed huge differences when different feedstock was used [13]. In summary, though large quantities of previous researches exist, the precise mechanisms of how soot properties are correlated to those reaction conditions are still mysterious due to the susceptible internal interactions happened in soot formation process.

To further understand the physicochemical mechanism of soot formation, plenty of studies have been carried out to inquire into the influential factors of soot properties. Trubetskaya et al. [19] studied the effect of different feedstock and pyrolysis temperatures on soot properties which are mainly nanostructure, and found out that high temperature and high content of potassium strongly influenced the soot reactivity in CO₂ gasification. Vander Wal and Tomasek [20] addressed the differences in soot nanostructure based upon formation and growth condition, stating a change between amorphous soot structure and a highly curved nanostructure when temperature, flow rate and fuel species changed. Böhm et al. [21] modeled the pyrolysis of acetylene and benzene at high temperatures and pressures and found a similar activation energy for high molecular PAH and soot formation, further concluding that soot mass growth rates were strongly related to PAH formation. However, with many studies investigating the soot formation mechanisms of biomass, coal and liquid or gaseous hydrocarbons, studies concentrating on soot products obtained from plastics are rare, among which studies on PU plastic are extremely lacking. What’s more, though few present studies [22, 23] have worked on soot formation of PU, the most common method adopted was combustion, and the soot was mainly generated in flame. Overall, the soot formation mechanism during PU pyrolysis under a relatively high temperature (> 1200 °C) is poorly understood.

To our knowledge, no previous efforts have been made to determine how the pyrolysis conditions including temperature and residence time influence PU pyrolysis soot product yield and soot properties. In this study, PU pyrolysis cases with different pyrolysis temperatures and residence times were carried out. The objective of this study is to determine the

effect of varied temperatures and residence times on product yield and soot properties including micro-morphology, physiochemical structure, surface functionality and oxidation reactivity. Based on the obtained knowledge, a specific soot formation pathway indicating soot formation mechanism during PU pyrolysis is suggested.

2. Materials and methods

2.1. Materials

Polyurethane used in this study was wasted PU plastic previously used as an insulation material inside refrigerators, collected from Croatia. The ultimate/proximate analyses and the ash composition analysis are shown in Table 1 and Table 2, respectively. PU samples contained high contents of oxygen (24.0 wt.%), nitrogen (6.4 wt.%) and volatile (83.2 wt.%), The Fe, Ti, Si, and Al contents were abundant in ash, and the sum of Na and K contents is 3.7 wt.%. Considering the samples were obtained from wasted foams, it is reasonable that PU samples were partly contaminated. The raw sample was first milled and sieved into the diameter of 50-100 μm , then dried at 105 °C for 24h in an oven before use.

Table 1. Ultimate and proximate analyses of polyurethane

Ultimate analysis (wt.%)					Proximate analysis (wt.%)		
C_{ad}	H_{ad}	O_{ad}	N_{ad}	S_{ad}	V_{ad}	FC_{ad}	A_{ad}
62.7	6.3	24.0	6.4	0.6	83.2	10.6	6.2

(V_{ad} : volatile matter as air dried basis; FC_{ad} : fixed carbon as air dried basis; A_{ad} : ash as air dried basis).

Table 2. Ash composition analysis

Sample	Fe_2O_3	TiO_2	SiO_2	CaO	ZnO	Al_2O_3	Na_2O	MgO	SO_3	BaO	K_2O	P_2O_5	CuO	Cl
Polyurethane	31.5	23.4	10.4	7.1	6.0	3.4	2.7	2.6	1.3	1.1	1.0	0.9	0.4	0.3

2.2. Experimental apparatus and procedure

2.2.1. Fixed-bed reactor

In this study, pyrolysis experiments were conducted in two fixed-bed reactor systems where different sets of reactors were adopted to realize different residence times of volatiles in the reactor tube. A longer quartz tube with length of 1500 mm was set in a large horizontal-chamber furnace to realize a long residence time of 2 s, a small one with length of 800 mm in a small furnace to realize a short residence time of 0.2 s. 2 s is the normal residence time of flue gas in the furnace, while 0.2 s is the lower limit we can control through the reactor and sampling probe design. The internal diameter of both quartz tubes was 30 mm. As shown in Fig. 1, from left to right are the nitrogen control unit, the temperature control unit, the quartz reactor unit, the soot collecting unit, the tar condensation unit, the gas filter and dryer unit, and the metering and analyzing unit.

The reactors were heated to target temperatures (1000, 1100, 1200, and 1300 °C) with the N₂ flow of 4 L min⁻¹ to create an inert atmosphere, and samples with a mass of 1 ± 0.005 g contained in a corundum boat were placed in the cool region of the reactor tube in N₂ atmosphere before experiments began. Below 1000 °C, there will be excessive tar in the reactor, adhering on the inner wall of reactor and sampling tube, which will significantly affect the accurate sampling of soot. 1300 °C is the upper limit at which the furnace can long-time run. After 30 min when a constant temperature and purely inert atmosphere (N₂ content > 99.9 wt.%) were obtained, the corundum was pushed into the constant-temperature reaction zone and rapidly pyrolyzed. The pyrolysis process of each sample lasted for 10 min which is an appropriate time that has proven to ensure the completion of total gas release. After that the quartz boat was pulled back to the cool region, cooled to room temperature in the N₂ atmosphere, and the solid residue was collected.

The soot collecting unit was heated to ~250 °C which was 50 °C higher than that in the work of Trubetskaya et al. [24] to avoid the condensation of tar products, and the soot collected was preserved for further characterization. The outlet of reactor was covered with PU materials for heat insulation to avoid overcooling of tar vapors, and the tar condensation unit consists of three tandem vessels containing dichloromethane cooled in the iced water to collect the condensable bio-oil. The volume of non-condensable gas was calculated when passing through a gas flow meter. A suitable amount of gas was separated by a three-way valve, collected by a gas bag and preserved. Each experiment was repeated two or three times to ensure the repeatability.

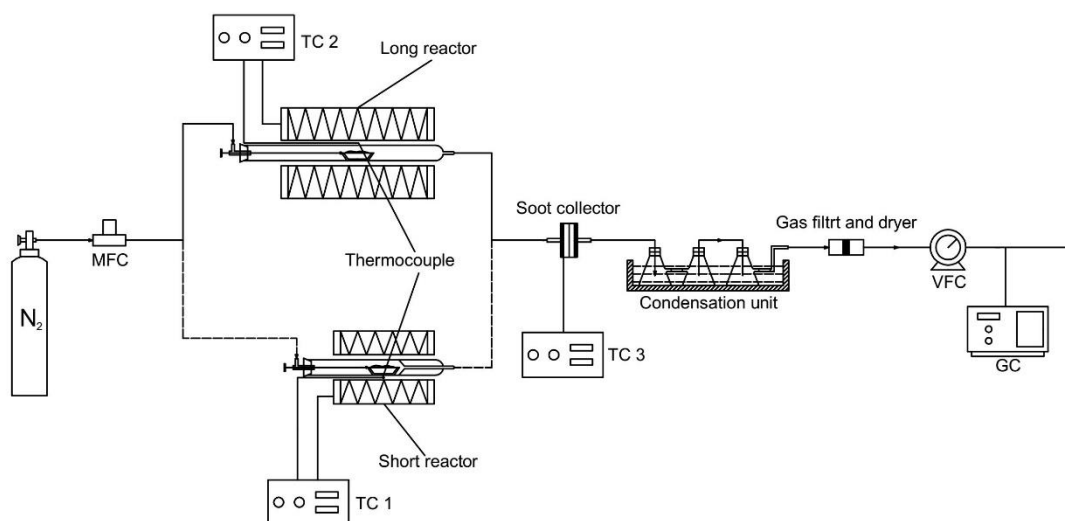


Fig. 1 Fixed-bed reactor system

2.2.2. Product yields measurement

The collected soot and char can be directly weighed by an electronic balance. The exhausted pyrolysis gases after condensation treatment, collected in gas bags, were then analyzed by a gas chromatograph (GC, GC-2014, Shimadzu, Japan) to quantify the concentrations of CO₂, CO, H₂, CH₄, and C₂H_m (C₂H₂, C₂H₄ and C₂H₆). Knowing the N₂ gas flow,

experimental time and gas concentration in the gas sample bags, the mass of other gases could be calculated, and the total gas yield could be further calculated. The quantity of the liquid fraction, including bio-oil and water, was calculated from the mass balance. The tar compositions were identified by a gas chromatograph-mass spectrometer (GC-MS, QP2010 Ultra, Shimadzu, Japan).

2.2.3. Soot characterization

Soot samples used for characterization analyses were first treated by ultrasonic extraction in dichloromethane solvent for 5 min, and then centrifugalized three times. Soot morphologies were observed by high-resolution transmission electron microscope (HR-TEM, JEM-2100, JOEL, Japan), and the crystal property was investigated by the X-ray diffraction (XRD, X'pert MPD Pro, PAN-alytical, Netherlands).

As a toxic pollutant, the oxidation reactivity of soot is important for its consumption and controlling. Therefore, the soot oxidation reactivity was investigated by thermogravimetric analyzer (TGA, STA-409PC, NETZSCH, German). For each test, approximately 5 mg of soot sample was placed in a corundum crucible and heated at a heating rate of 20 K min⁻¹ from room temperature to 1273 K in air atmosphere environment (20 vol.% O₂/80 vol.% N₂) with a total flow rate of 100 ml min⁻¹. All tests were performed under the same conditions to guarantee the comparability. The mass loss (TG) curves and differential thermogravimetric (DTG) curves were online-recorded.

3. Results and discussion

3.1. Soot, gas, char and tar yields

The yield of soot/gas/tar/char products as pyrolysis temperature varied in 1000-1300 °C with different residence times were illustrated in Figs. 2(a) and 2(b), respectively. With a residence time of ~2 s, as shown in Fig. 2(a), a soot yield of 11.1 wt.% was obtained under 1000 °C. An obvious positive correlation can be observed between increasing temperature from 1000 °C to 1300 °C and soot yield which reached to 24.5 wt.% under highest temperature. This result coincides well with some previous studies [25, 26] that have concluded the increasing temperature strengthened the thermal cracking and decomposition reactions of heavy hydrocarbons in tar into lighter radicals, and these radicals (mainly C₂-C₆ compounds) were then polymerized and formed PAH compounds, and functioned in soot formation process. Note that some simultaneous interactions happening along with soot nucleation and surface growth which were the reason to soot quantity increase, that is, thermal cracking of soot chemical structures and partial oxidation by oxygen-containing radicals (-OH, -C=O-, etc.), might be contributions to potential soot quantity decrease when temperature continuously rises [27]. Considering the high content of oxygen in PU samples which is 24.01 wt.% as shown in Table 1 and the relatively high contents of CO/CO₂ in pyrolysis gases, these negative reactions for soot formation might not be neglected.

Flecher et al. [17] have stated a favored polymerization reaction over cracking and oxidation reactions when soot formed lower than 2000 K, promising the increase of soot in quantity.

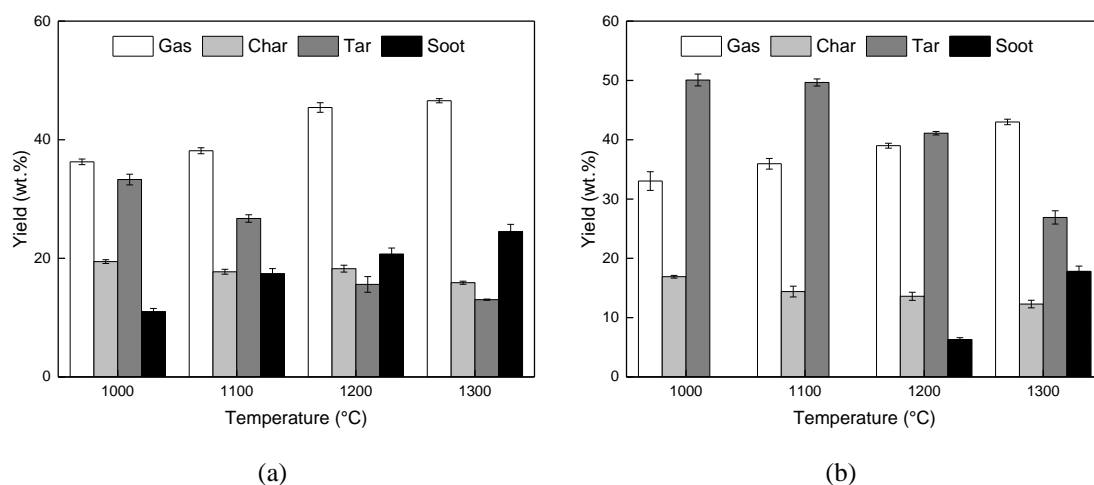


Fig. 2 The effect of pyrolysis temperature on product yields: (a) residence time-2s; (b) residence time-0.2s.

In Fig. 2(a), the tar yield is observed to decrease from 33.3 wt.% at 1000 °C to 19.0 wt.% at 1300 °C, which corresponds well with the explanation above, that the reduction of tar content is mainly ascribed to the instability of heavy hydrocarbons under relatively high temperatures. The majority of primary hydrocarbon compounds in pyrolysis volatiles are aliphatic and aromatic hydrocarbons, according to Chen et al. [28], aliphatic compounds are unstable under high temperature and are easily broken into small molecules, while aromatic ring structures are relatively stable and tends to polymerize into PAHs. The broken molecular radicals then incline to develop into small gaseous components that lead to an increase in gas yield, part of which also participates in soot formation [29]. The yield of pyrolysis gas increases from 36.3 wt.% at 1000 °C to 40.6 wt.% at 1300 °C. A slight change from 19.5 wt.% at 1000 °C to 15.9 wt.% at 1300 °C is observed in char yield when temperature increases. This is mainly due to the limited volatile content in PU samples that can be released during pyrolysis. In summary, increasing temperature enhances thermal cracking of raw PU samples and slightly increases the release of volatiles, leading to a slight decrease in char yield. Higher temperature enhances the reforming and decomposition of volatile species and thus brings about decreased tar yield, and increases light gases and hydrocarbons.

Fig. 2(b) shows the distributions of pyrolysis products obtained under increasing temperature with a shorter residence time of 0.2 s. By comparison, it can be observed that the changing trends of pyrolysis products as the temperature increasing between pyrolysis cases with long and short residence times are similar, however, the product yield distributions are different. As shown in Fig. 2(b), soot only forms when temperature increases to 1200 °C which is a much higher initial temperature of soot occurrence compared to that in Fig. 2(a) with a longer residence time of 2 s. At 0.2 s, the soot and gas yields are lower than those in the pyrolysis with a longer residence time, while the tar yield is

significantly higher. This can be ascribed to the limited residence time in the high temperature region of the released volatiles from PU samples, and thus the thermal cracking and decomposition reactions of volatile compounds were deficient. After undergoing secondary reactions of volatiles at high temperatures, small PAH compounds grow into larger ones of molecular weights 500-1000. Condensation begins when the PAHs grow to the size of four rings and larger, collision giving birth to the formation of small clusters. The simultaneous condensation and the PAH growth finally lead to the formation of soot particles, or described as 'soot precursor'. Consequential lack of intermediate, accompanied with insufficient reacting time for volatile secondary reactions directly leads to significantly declines in soot yield which highly relies on the grow from PAHs to soot precursor, and in gas yield which is mainly dominated by the breaking of large hydrocarbons into small molecular radicals and further development into small molecular gas species [28]. The minor difference between char products at different volatile residence times, that is, the yield of char obtained from longer residence time is slightly higher than that from shorter residence time. It can be explained by the sorption of volatile organic compounds due to the micro-porous structure and abundant surface functional groups of char itself [30, 31]. A longer volatile residence time means more contact between char and volatiles, more sorption of organic compounds and thus higher weight.

3.2. Soot characterization

3.2.1. Soot micro-morphologies

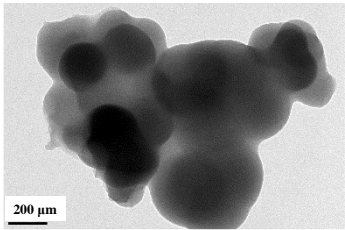
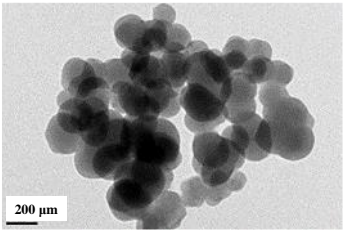
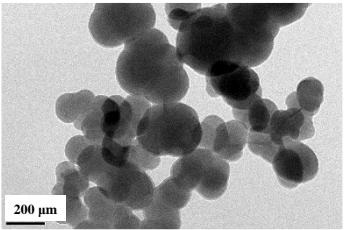
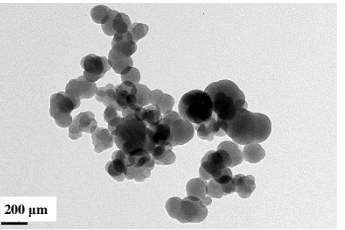
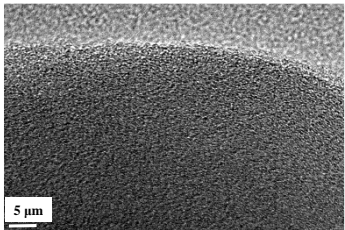
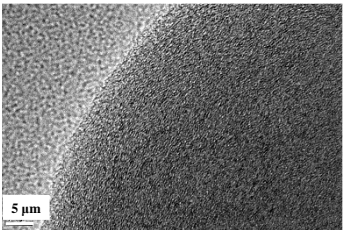
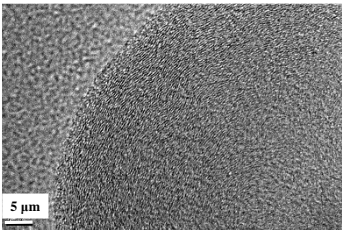
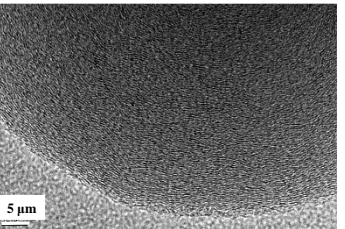
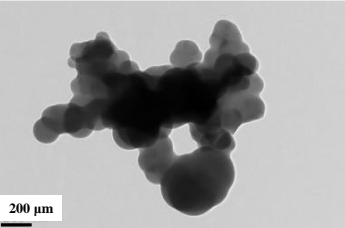
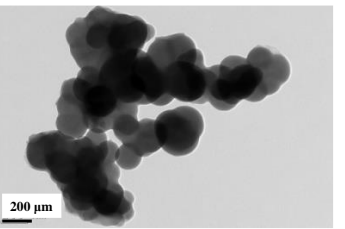
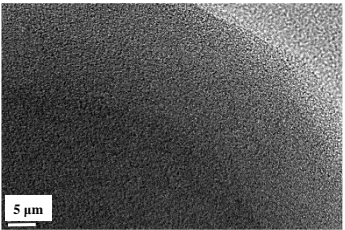
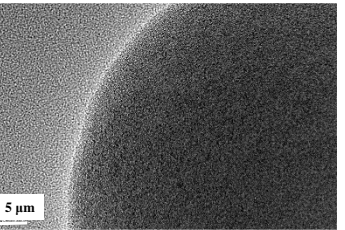
The micro-morphologies of soot particles collected under different temperatures and residence times were obtained by HR-TEM, as shown in Table 3. At a residence time of 2 s, the soot collected from pyrolysis at 1000 °C consists of primary particles whose diameters ranged from 200-500 nm, indicating the morphologies of an aggregated cluster in irregular shapes with diameters of 1-2 μm. Surrounding the particles of spherical nuclei agglomerating together are structures with higher transparency in TEM images that show smooth edges and curved surfaces. Similar results were obtained from both TEM and AFM by Abid et al. [18] who used 'halo' to define the coating structures, indicating that the particles were not solid but liquid-like tar-balls, and under the impact of TEM substrate they would spread over the surface. This morphology implies the unfinished carbonization process during which the liquid-like precursor particles solidified, involving the conversion of PAH contents with high hydrogen mole fraction to highly carbonized ones. As comparison, the soot particles from pyrolysis at 1100 °C and 1200 °C are much better-defined with smaller sizes (50-200 nm) but still contain a certain number of larger irregular particles (~200 nm). When temperature reaches 1300 °C, a large portion of irregular large particles disappear, while larger amounts of regular, distinct spherical-boundary fine particles (30-150 nm) dominate. When comparing the enlarged views of soot particles obtained under these four temperatures, the stacking of the graphite layers results in disordered internal structures as observed from images of soot particles at

1000 °C and 1100 °C, while regular soot structures with parallel, ordered graphite layers around a core, i.e., onion-like structures, can be distinguished at 1200 °C and 1300 °C. Hence, it can be concluded that a higher temperature contributes to an enhanced soot carbonization degree.

Morphologies of soot particles also significantly changed when the volatile residence time changes from 2 s to 0.2 s, as shown in Table 3. At the same pyrolysis temperatures, soot particles obtained from the case of 0.2 s show much more disordered and liquid-like surfaces which indicated inadequate development and carbonization, compared to those from pyrolysis case of 2 s. This means the shorter residence time impaired the positive effect of high temperature on soot formation and development, resulting in that the soot particles at high temperatures and the short volatile residence time showed similar morphologies with those at lower temperatures and the long volatile residence time. This phenomenon might be ascribed to two reasons: (1) the shorter residence time weakens the decomposition and cracking process of volatile compounds, thereby produces less active radicals attached on soot surfaces, and diminishes the contact between soot precursor and the volatile species, thus generating agglomerates consisting of nascent soot particles instead of well-developed soot particles [32]; (2) the shorter residence time of soot in high temperature environment directly restricts the carbonization process of soot particles [33].

1

Table 3 Micro-morphologies of nano-scale soot particles produced at varied temperatures and residence times

Residence time	Pyrolysis temperature	1000 °C	1100 °C	1200 °C	1300 °C
~2s	Scale=200 nm				
	Scale=5 nm				
~0.2s	Scale=200 nm	None	None		
	Scale=5 nm	None	None		

3.2.2. XRD patterns

XRD patterns of soot particles obtained in the temperature range of 1000-1300 °C are characterized and shown in Fig. 3. The broad reflections at 24.2° and 43.3° indicate the development of a crystalline phase which is assigned to the parallel graphite layers, representing the highly carbonized onion-like soot structure observed in TEM morphologies. Similar results have been reported by Trubetskaya et al. [19] who claimed that the reflection at 25° spaced at a well-defined inter-planar distance represented the parallel graphene layers while the reflection at 43.6° representing two-dimensional reflections indicating the ordering of carbon atoms inside the graphite layers. It can be seen from Fig. 3 that the featured peak height significantly increases when temperature increases from 1000 °C to 1100 °C, and from 1100 °C to 1200 °C as well, however, this increase is very modest when temperature increases from 1200 °C to 1300 °C. This result agrees well with the morphologies by TEM, indicating that 1100 °C is a critical temperature when the graphite layer structures begin to occur and develop.

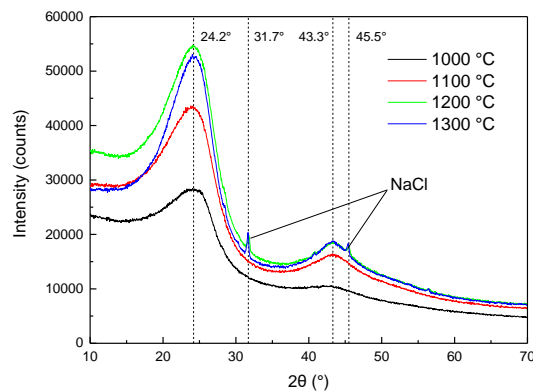
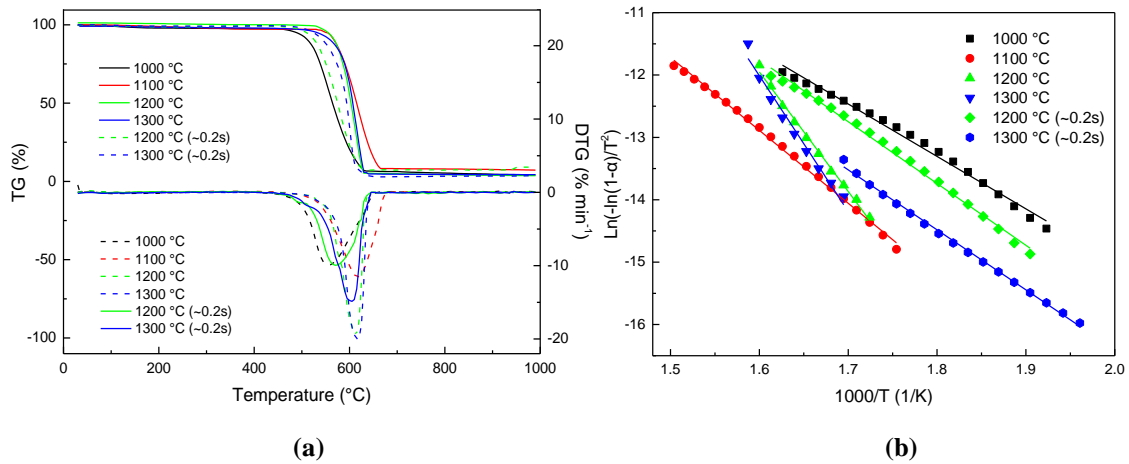


Fig. 3 XRD analysis of soot particles from 1000-1300 °C.

Besides the obvious reflections at 24.2° and 43.3°, two small sharp peaks are also observed at 31.7° and 45.5°, respectively, only at 1200 °C and 1300 °C. The XRD analysis indicates that these two peaks represent the existence of NaCl in soot particles. The selectively occurrence of NaCl in relatively high temperatures indicates that the Na in plastic waste at high temperatures can evaporate and combine with Cl to form NaCl molecular, and then condensed into NaCl crystals with the temperature decreasing. Li et al [34] has reported the increasing release of gaseous potassium with increasing temperature, indicating a similar release mechanism of metal species at high temperatures. Di Stasio et al. [35] and Trubetskaya et al. [19] have reported the inhibition of coagulation and agglomeration of soot particles due to charge exchange with the existence of alkali and alkaline earth metallic species (AAEMs). This statement highly agreed with the result of TEM where soot particles from 1200 °C and 1300 °C showed evidently smaller particle sizes and less agglomeration property, as shown in Table 3.

3.2.3. Soot reactivity

26 The oxidation reactivity of soot is important for the control of trace soot emission during incineration process, as well as
 27 the performances of soot products used in different industries. In this part, the oxidation reactivity of soot in air
 28 atmosphere environment of 20 vol.% O₂/80 vol.% N₂ was tested by a non-isothermal TGA. The measured TG-DTG
 29 curves and Arrhenius kinetic plotting are shown in Fig. 4, and the characteristic parameters are summarized in Table 4,
 30 where T_s (°C) is the start temperature of soot oxidation, T_{peak} (°C) is the peak temperature of DTG curves, T_f (°C) is the
 31 finish temperature of soot oxidation, w_{max} is the maximum mass loss rate or the peak height of DTG curves, E (kJ mol⁻¹)
 32 is the apparent activation energy and A (s⁻¹) is the pre-exponential factor of soot oxidation. The definition methods of
 33 these characteristic parameters can be found in our previous work [36].



34
 35
 36 **Fig. 4 (a) TG-DTG curves and (b) Arrhenius plotting of soot oxidation.**

37 As shown in Fig. 4(a), when the pyrolysis temperature increases from 1000 °C to 1100 °C, TG-DTG curves significantly
 38 shifted right with T_i , T_{peak} , and T_f increasing by 49 °C, 58 °C, and 38 °C, respectively. However, while the pyrolysis
 39 temperature further increases from 1100 °C to 1200 °C, T_i decreases by 11 °C, T_{peak} showing no change and T_f even
 40 decreasing by 22 °C, which results in a more drastic mass loss ratio. When the pyrolysis temperature increased from
 41 1200 °C to 1300 °C, TG-DTG curves slightly shift right, and these three characteristic temperatures increased by 3-7 °C.
 42 As for the mass loss rate or kinetic parameters, shown in Table 4, with the increase of pyrolysis temperature in the range
 43 of 1000-1300 °C, the increases of w_{max} , E , and A can be observed. When the pyrolysis temperature increases to the range
 44 of 1200-1300 °C, the apparent activation energy is relatively stable at the range of 159-181 kJ mol⁻¹.

45 The measured results of soot oxidation reactivity at different pyrolysis temperatures can be explained by the
 46 micro-morphologies of soot particles introduced in Table 3. (1) At 1000 °C, particles exist as liquid-like phase but with
 47 much larger diameters than those produced at higher temperatures, which results in much lower characteristic
 48 temperatures and higher oxidation reactivity. The composition of those not well carbonized soot particles is complex with
 49 a relatively low contents of carbon [20], some components in which require a high temperature to burn out, contributing

50 to a wide distribution of DTG peak, in respect to a heterogeneous soot mixture with varied compositions and particle size
51 distribution [37]. (2) Pyrolysis temperature increasing to 1100 °C gives birth to a large amount of well-developed,
52 spherical solid-phase finer soot particles with developed, more aromatic hydrocarbon structures which are much more
53 difficult than liquid-like particles to be oxidized [38]. On the other hand, there are still a non-negligible number of
54 liquid-like particles. This demonstrates the reason of DTG curve of soot sample of 1100 °C maintaining a wide
55 distribution and a modest mass loss rate. (3) When the pyrolysis temperature increases to 1200 °C and 1300 °C, the soot
56 particles dominantly exist in the form of nanoscale soot particles with ordered and relatively fine sizes and uniform
57 chemical compositions, while those disordered large liquid-like particles with complicated compositions almost
58 disappeared, leading to a decreased finish temperature.

59 Additionally, another important factor affecting the performances of soot oxidation is the existence of NaCl in soot
60 products. XRD patterns in Fig. 3 have proved the existence of NaCl in soot particles from PU pyrolysis at higher than
61 1100 °C, which might play the role of catalyst during soot oxidation process. According to Neeft et al. [39], the intensity
62 of contact between soot and alkali metals is a major predictor of soot oxidation rate. Thus, the resulted salience of soot
63 samples from 1200 °C and 1300 °C in significantly higher oxidation reactivity, indicated by the left-shifting TG curves
64 and promoted DTG peaks, explained by possible catalytic effect, was reasonable. Similar result has been observed in the
65 work of Wang et al. [36].

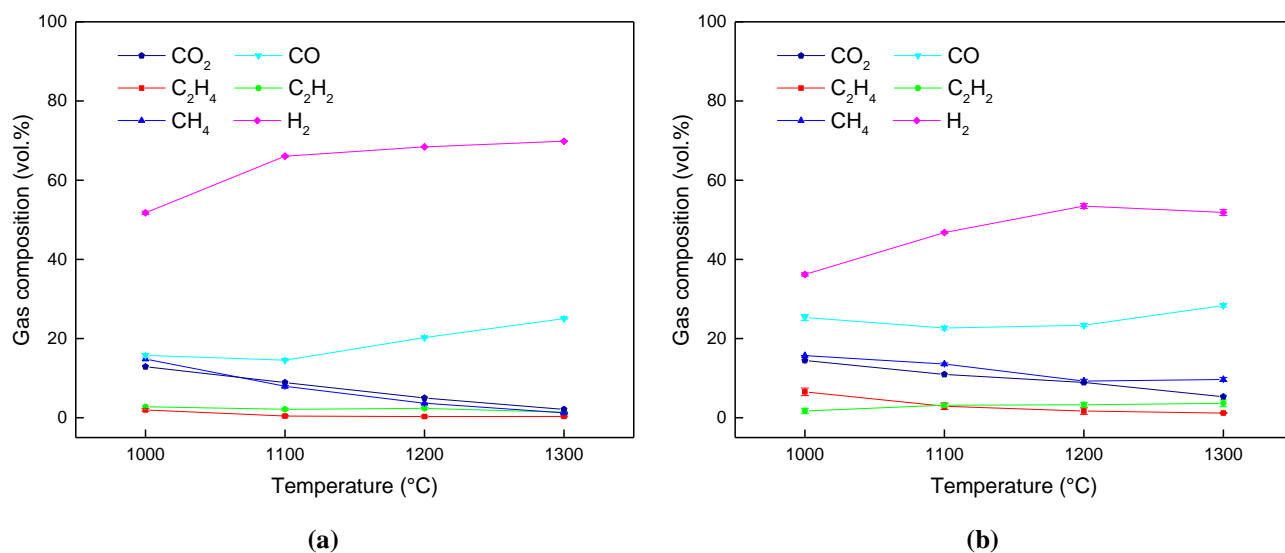
66 When pyrolysis was conducted at a shorter residence time of 0.2 s, the soot products obtained at 1200 °C and 1300 °C
67 showed relatively higher oxidation reactivity compared with those with a residence time of 2 s. As listed in Table 4, with
68 the same pyrolysis temperature, these characteristic parameters of soot oxidation at 0.2 s are all lower than those at 2 s.
69 This result aligns well with the morphology results in Table 3, that the soot particles produced at the shorter residence
70 time are more liquid-like, indicating a better oxidation reactivity.

71 **Table 4** The summary of characteristic parameters in all studied cases.

Residence time s	Pyrolysis temperature °C	T_i °C	T_{peak} °C	T_f °C	w_{max} %/min	E kJ mol ⁻¹	A 1/s	R^2 1
2	1000	518	559	614	9.9	69.9	521.6	0.923
	1100	567	617	652	11.6	97.1	38812	0.993
	1200	578	617	630	19.5	159.3	2.5E10	0.991
	1300	585	620	634	20.2	181.1	1.8E12	0.992
0.2	1200	521	580	613	9.6	82.6	5595	0.973
	1300	532	602	634	14.8	80.2	1586	0.997

72 **3.3. Gas composition**

73 The compositions of pyrolysis gases and their distribution changes with increasing temperature at two residence times are
 74 shown in Figs. 5(a) and 5(b), respectively. From Fig. 5(a), a dominant amount of H₂ content which is 51.7 vol.% at
 75 1000 °C and 69.8 vol.% at 1300 °C can be observed. This abundance of H₂ in pyrolysis gases was mainly due to the
 76 facilitated cyclization and aggregation reactions when temperature increases during soot formation and growth. The
 77 small molecules not only attach to the surface of soot particles but also join to each other and formed small aromatic
 78 compounds at the cost of release of H atoms, and further formation of H₂, known as hydrogen abstraction [29]. The slight
 79 decrease of CH₄, C₂H₂ and C₂H₄ contents match well with this explanation. The CO content increases from 15.8 vol.% at
 80 1000 °C to 25.0 vol.% at 1300 °C, while on the contrary the content of CO₂ decreases from 12.9 vol.% at 1000 °C to 2.1
 81 vol.% at 1300 °C. This result can be mainly explained by the facilitated oxidation of soot when temperature increases.
 82 Along with other oxidative radicals, CO₂ in gas phase might play an important role as oxidant at high temperature,
 83 partially oxidizing soot particles, leading to a decrease in CO₂ content but an increase in CO content.
 84 Fig. 5(b) shows the gas compositions at a shorter volatile residence time of 0.2s. Similarity in the developing trend of
 85 same gaseous species to that in Fig. 5(a) is observed, while the content of each component is not completely consistent.
 86 When pyrolysis happens at the same temperature, a lower H₂ content as well as a higher CO content at a shorter
 87 residence time can be observed, while other components show only marginal increase. This was mainly due to the
 88 diminished secondary reactions in volatile phase that inhibit the hydrogen abstraction reaction and further H₂ release,
 89 resulting in the consequent decrease of H₂ content and increase of other gas species' contents.



90 **Fig. 5 The effect of pyrolysis temperature on gas product compositions: (a) 2 s; (b) 0.2 s.**

91 **3.4. PAHs in tar products**

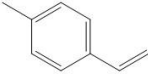
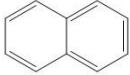
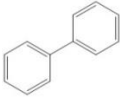
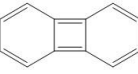
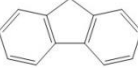
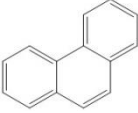
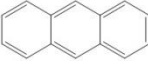
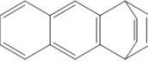

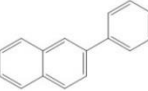

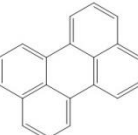


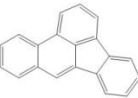
92 The detectable compounds in tar from PU pyrolysis at temperature of 1000-1300 °C are listed in Table 5, and
 93 summarized in Table 6 in terms of 'aromatic ring number' to determine the development of PAH compounds. The

94 generally expected liquid product should be a very complex mixture of organic compounds containing mainly aromatic
95 compounds as well as noticeable aliphatic compounds and heterocyclic nitrogen-containing and oxygen-containing
96 species [40]. However, at the relatively high pyrolysis temperature in this study, only trace amount of those
97 nitrogen-containing and oxygen-containing compounds are detected. Herrera et al. [41] reported further decompose of
98 PU samples to smaller compounds and the release of nitrogen content in the form of nitrogen-containing products like
99 HCN, acetonitrile, etc. Zhang et al. [2] adopted a model compound method to investigate the thermal degradation of PU
100 materials and found out the thermal breaking of C-O and C-N bonds during pyrolysis. Therefore, the absence of
101 heterocyclic compounds in tar can be mainly attributed to the breaking of C-O and C-N bonds at such high temperatures
102 and the release of small molecular gaseous compounds (CO, CO₂, NO_x, HCN, etc.) [42]. The disappearance of aliphatic
103 compounds, according to our previous research [13], is mainly a result of high temperature and long volatile residence
104 time.

105 A significant decrease in the amount of tar species can be observed from Table 5 when the pyrolysis temperature
106 increases. This change implies that the temperature increasing enhances the depolymerization and aromatization
107 reactions of volatile compounds, resulting in the transformation from higher reactivity compounds to highly
108 thermal-stable PAHs, such as perylene, benzo[e]pyrene, naphthacene, etc. This trend is clearly exhibited in Table 6
109 where the distribution of tar composition ring numbers is highly related to the pyrolysis temperature [13]. In the studied
110 temperature range, at 1000 °C and 1100 °C, the species of ring number ≥ 5 are rarely observed in tar products, and the tar
111 composition is dominated by the species of ring number ≤ 4 . However, when the pyrolysis temperature increases to
112 1200 °C and 1300 °C, the overall content of species of ring number ≥ 4 becomes over 50 wt.%.

113

Table 5 Tar compositions at varied pyrolysis temperatures (1000-1300 °C)

No.	Compound	Formula	Structural formula	1000 °C	1100 °C	1200 °C	1300 °C
1	Benzene,-1-ethenyl-4-methyl-	C ₉ H ₁₀		-	0.97	-	-
2	Naphthalene	C ₁₀ H ₈		15.13	-	-	-
3	Biphenyl	C ₁₂ H ₁₀		1.27	-	-	-
4	Biphenylene	C ₁₂ H ₈		12.57	2.27	-	-
5	Fluorene	C ₁₃ H ₁₀		1.42	-	-	-
6	Phenanthrene	C ₁₄ H ₁₀		24.3	14.81	-	5.34
7	Anthracene	C ₁₄ H ₁₀		-	2.8	10.23	0.94
8	1,4-Ethenoanthracene, -1,4-dihydro-	C ₁₆ H ₁₂		-	-	-	1.92
9	4H-Cyclopenta[def]p henanthrene	C ₁₅ H ₁₀		1.36	1.95	-	-
10	Naphthalene,-2-pheny l-	C ₁₆ H ₁₂		0.93	0.48	-	-
11	Fluoranthene	C ₁₆ H ₁₀		22.60	54.49	11.04	-
12	Perylene	C ₂₀ H ₁₂		-	-	42.23	-
13	Benzo[e]pyrene	C ₂₀ H ₁₂		-	0.69	-	32.45
14	Pyrene	C ₁₆ H ₁₀		-	-	-	0.78
15	Benz[e]acephenanthry lene	C ₂₀ H ₁₂		-	-	-	7.43


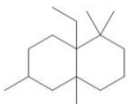
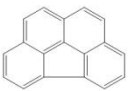
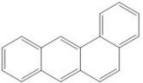

16	Benzo[c]phenanthrene	C ₁₈ H ₁₂		-	0.38	-	-
17	Benzo[ghi]fluoranthene	C ₁₈ H ₁₀		5.16	20.09	-	-
18	Benz[a]anthracene	C ₁₈ H ₁₂		-	0.57	10.54	-
19	Naphthacene	C ₁₈ H ₁₂		1.7	-	-	1.12
20	Triphenylene	C ₁₈ H ₁₂		2.29	-	3.53	10.24

Table 6. Tar composition profiles by 'ring number' at 1000-1300 °C

Aromatic ring number	1000 °C	1100 °C	1200 °C	1300 °C
1	0.00	0.97	0.00	0.00
2	30.39	0.00	0.00	0.00
3	49.19	20.36	21.27	8.2
4	3.99	57.39	14.07	19.57
≥5	0.00	0.00	42.23	32.45

3.5. Pathway of soot formation during PU pyrolysis at high temperatures

Based on the above characterization results of soot, gas and tar products, a reaction pathway of soot formation during PU pyrolysis at high temperatures is proposed in Fig. 6. When undergoing thermal cracking at high temperatures, the molecular structures of polyurethane polymer start to break down and 4,4'-diphenylmethane diisocyanate, considered as the dominant intermediate during prior cracking process. Subsequently the scission of carbon-nitrogen and carbon-oxygen bonds occurs [2], 4,4'-diphenylmethane diisocyanate degrading into 4,4-diaminodiphenyl methane with the release of CO and CO₂ gases.

Then after undergoing secondary reactions in the form of volatiles in the high temperature region of the reactor, small PAH compounds with 1-5 aromatic rings grow into larger PAHs of molecular weights 500-1000 via the interactions known as HACA mechanism [15] and "ring-ring condensation" interaction (under sufficient aromatic species concentration only) [16]. It is worth noting that the two pathways are not isolated but co-constructing to build up the PAHs growth mechanism. Condensation begins when the PAHs grow to the size of four rings and larger, collision giving birth to the formation of small clusters. The simultaneous condensation and the PAH growth finally lead to the formation of soot particles, or described as 'soot precursor'. This process is known as particle inception [17, 18, 43].

131 The development of soot after the particle inception is mainly dominated by: (1) the surface growth in which gas-phase
132 species are attached to the surface of a particle, leading to an increase of soot amount without changing particle numbers,
133 and (2) coagulation where particles collide and coalesce, leading to the decrease of number density. Remarkably, only 10
134 wt.% of the soot mass is produced during the inception period whereas as much as 90 wt.% of the total comes from
135 surface growth [43]. At final stages, the discernable primary particles are chemically fused together, known as
136 agglomerate. The morphology of soot particles, whose diameters are about 20-100 nm, in terms of chains, clusters,
137 dendrites, rings, spheroids, flakes and other types, is observed.

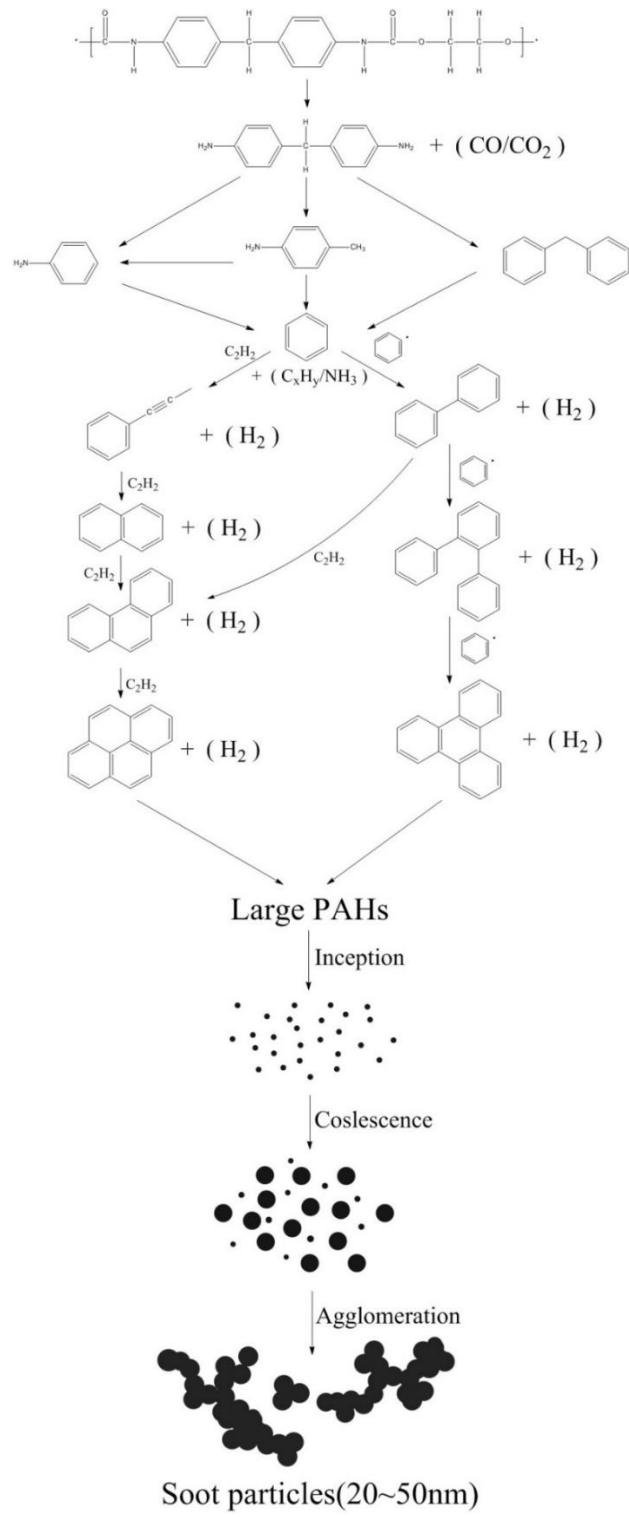


Fig. 6 The formation pathway of soot during PU pyrolysis.

138

139

140 **4. Conclusions**

141 (1) The initialization and growth of soot particles during PU pyrolysis requires a certain high temperature and long
 142 volatile residence time. With a volatile residence time of 2 s, the soot yield is 11.0 wt.% at 1000 °C and increases to
 143 24.5 wt.% when the pyrolysis temperature increases to 1300 °C. In contrast, with a short volatile residence time of

144 0.2 s, the soot cannot be observed until 1200 °C. The increase of pyrolysis temperature increases the soot and gas
145 yields while decreases the tar and char yields. The decrease of volatile residence time decreases the soot, gas and
146 char yields while increases the tar yield. The soot formation pathway during PU pyrolysis at higher temperatures can
147 be reflected by the gas and tar composition measurement.

148 (2) The soot morphology and reactivity are significantly affected by the pyrolysis temperature and volatile residence
149 time. More carbonized and ordered structures with distinguishable parallel graphitic layers are observed in the soot
150 particles produced from higher temperature or longer residence time. The temperature about 1100 °C is a critical
151 temperature for soot formation, beyond which the parallel layered structures begin to form. When the volatile
152 residence time decreases from 2 s to 0.2 s, the oxidation reactivity of soot decreases. The NaCl coexisting with soot
153 is observed by XRD when the pyrolysis temperature increases from 1100 °C to 1200 °C, which catalytically
154 promotes the soot oxidation.

155 **Acknowledgements**

156 The authors gratefully acknowledge the financial support of the National Natural Science Foundation of China (Nos.
157 51676157 and 5161101654), and the National Key Research and Development Program of China (No. 2017YFB0603902).

158 **References**

159 [1] F. Pinto, P. Costa, I. Gulyurtlu, I. Cabrita. Pyrolysis of plastic wastes. 1. Effect of plastic waste composition on product
160 yield. *Journal of Analytical & Applied Pyrolysis*. 51 (1999) 39-55.

161 [2] Y. Zhang, Z. Xia, H. Huang, H. Chen. Thermal degradation of polyurethane based on IPDI. *Journal of Analytical and*
162 *Applied Pyrolysis*. 84 (2009) 89-94.

163 [3] W.R. Lea. Plastic incineration versus recycling: a comparison of energy and landfill cost savings. *Journal of Hazardous*
164 *Materials*. 47 (1996) 295-302.

165 [4] C. Achillas, C. Vlachokostas, N. Moussiopoulos, G. Baniyas, G. Kafetzopoulos, A. Karagiannidis. Social acceptance for
166 the development of a waste-to-energy plant in an urban area. *Resources, Conservation and Recycling*. 55 (2011) 857-63.

167 [5] R. Siddique, J. Khatib, I. Kaur. Use of recycled plastic in concrete: A review. *Waste Management*. 28 (2008) 1835-52.

- 168 [6] M. Kanniche, R. Gros-Bonnivard, P. Jaud, J. Valle-Marcos, J.-M. Amann, C. Bouallou. Pre-combustion,
169 post-combustion and oxy-combustion in thermal power plant for CO₂ capture. *Applied Thermal Engineering*. 30 (2010)
170 53-62.
- 171 [7] A.V. Bridgwater. Review of fast pyrolysis of biomass and product upgrading. *Biomass and bioenergy*. 38 (2012) 68-94.
- 172 [8] W. Kaminsky, J.-S. Kim. Pyrolysis of mixed plastics into aromatics. *Journal of Analytical and Applied Pyrolysis*. 51
173 (1999) 127-34.
- 174 [9] K. Crombie, O. Mašek. Investigating the potential for a self-sustaining slow pyrolysis system under varying operating
175 conditions. *Bioresource technology*. 162 (2014) 148-56.
- 176 [10] G. Ruoppolo, P. Ammendola, R. Chirone, F. Miccio. H₂-rich syngas production by fluidized bed gasification of
177 biomass and plastic fuel. *Waste Management*. 32 (2012) 724-32.
- 178 [11] W. Buss, O. Mašek, M. Graham, D. Wüst. Inherent organic compounds in biochar—Their content, composition and
179 potential toxic effects. *Journal of Environmental Management*. 156 (2015) 150-7.
- 180 [12] S.D.A. Sharuddin, F. Abnisa, W.M.A.W. Daud, M.K. Aroua. A review on pyrolysis of plastic wastes. *Energy*
181 conversion and management. 115 (2016) 308-26.
- 182 [13] Q. Jin, X. Wang, S. Li, H. Mikulčić, T. Bešenić, S. Deng, et al. Synergistic effects during co-pyrolysis of biomass and
183 plastic: gas, tar, soot, char products and thermogravimetric study. *Journal of the Energy Institute*. (2017).
- 184 [14] V. Hall-Roberts, A. Hayhurst, D. Knight, S. Taylor. The origin of soot in flames: Is the nucleus an ion? *Combustion*
185 and flame. 120 (2000) 578-84.
- 186 [15] B. Öktem, M.P. Tolocka, B. Zhao, H. Wang, M.V. Johnston. Chemical species associated with the early stage of soot
187 growth in a laminar premixed ethylene–oxygen–argon flame. *Combustion and Flame*. 142 (2005) 364-73.

188 [16] H. Böhm, H. Jander, D. Tanke. PAH growth and soot formation in the pyrolysis of acetylene and benzene at high
189 temperatures and pressures: Modeling and experiment. Symposium (International) on Combustion. Elsevier 1998. pp.
190 1605-12.

191 [17] T.H. Fletcher, J. Ma, J.R. Rigby, A.L. Brown, B.W. Webb. Soot in coal combustion systems. Progress in Energy and
192 Combustion Science. 23 (1997) 283-301.

193 [18] A.D. Abid, N. Heinz, E.D. Tolmachoff, D.J. Phares, C.S. Campbell, H. Wang. On evolution of particle size
194 distribution functions of incipient soot in premixed ethylene–oxygen–argon flames. Combustion and Flame. 154 (2008)
195 775-88.

196 [19] A. Trubetskaya, P.A. Jensen, A.D. Jensen, A.D.G. Llamas, K. Umeki, D. Gardini, et al. Effects of several types of
197 biomass fuels on the yield, nanostructure and reactivity of soot from fast pyrolysis at high temperatures. Applied Energy.
198 171 (2016) 468-82.

199 [20] R.L. Vander Wal, A.J. Tomasek. Soot nanostructure: dependence upon synthesis conditions. Combustion and Flame.
200 136 (2004) 129-40.

201 [21] H. Böhm, H. Jander, D. Tanke. PAH growth and soot formation in the pyrolysis of acetylene and benzene at high
202 temperatures and pressures: Modeling and experiment. Symposium (International) on Combustion. 27 (1998) 1605-12.

203 [22] C. Branca, C. Di Blasi, A. Casu, V. Morone, C. Costa. Reaction kinetics and morphological changes of a rigid
204 polyurethane foam during combustion. Thermochimica Acta. 399 (2003) 127-37.

205 [23] J.-H. You, P.-C. Chiang, K.-T. Chang, S.-C. Chang. Polycyclic aromatic hydrocarbons (PAHs) and mutagenicity of
206 soot particulates in air emissions from two-stage incineration of polystyrene. Journal of hazardous materials. 36 (1994)
207 1-17.

208 [24] A. Trubetskaya, P.A. Jensen, A.D. Jensen, A.D. Garcia Llamas, K. Umeki, P. Glarborg. Effect of fast pyrolysis
209 conditions on biomass solid residues at high temperatures. Fuel Processing Technology. 143 (2016) 118-29.

210 [25] A.V. Krestinin. Detailed modeling of soot formation in hydrocarbon pyrolysis. *Combustion and Flame*. 121 (2000)
211 513-24.

212 [26] P.A. Vlasov, J. Warnatz. Detailed kinetic modeling of soot formation in hydrocarbon pyrolysis behind shock waves.
213 *Proceedings of the Combustion Institute*. 29 (2002) 2335-41.

214 [27] Y. Sivathanu, J. Gore. Coupled radiation and soot kinetics calculations in laminar acetylene/air diffusion flames.
215 *Combustion and Flame*. 97 (1994) 161-72.

216 [28] L. Chen, X. Zhang, L. Sun, H. Xu, H. Si, N. Mei. Study on the Fast Pyrolysis of Oil Sludge and Its Product Distribution
217 by PY-GC/MS. *Energy & Fuels*. 30 (2016) 10222-7.

218 [29] M. Frenklach. Reaction mechanism of soot formation in flames. *Physical Chemistry Chemical Physics*. 4 (2002)
219 2028-37.

220 [30] W. Buss, O. Mašek. High-VOC biochar—effectiveness of post-treatment measures and potential health risks related to
221 handling and storage. *Environmental Science and Pollution Research*. 23 (2016) 19580-9.

222 [31] A. Budai, L. Wang, M. Gronli, L.T. Strand, M.J. Antal, S. Abiven, et al. Surface Properties and Chemical Composition
223 of Corncob and Miscanthus Biochars: Effects of Production Temperature and Method. *Journal of Agricultural and Food*
224 *Chemistry*. 62 (2014) 3791-9.

225 [32] S. Septien, S. Valin, M. Peyrot, C. Dupont, S. Salvador. Characterization of char and soot from millimetric wood
226 particles pyrolysis in a drop tube reactor between 800°C and 1400°C. *Fuel*. 121 (2014) 216-24.

227 [33] L.G. Blevins, R.A. Fletcher, B.A. Benner, E.B. Steel, G.W. Mulholland. The existence of young soot in the exhaust of
228 inverse diffusion flames. *Proceedings of the Combustion Institute*. 29 (2002) 2325-33.

229 [34] H. Li, K. Han, Q. Wang, C. Lu. Influence of Ammonium Phosphates on Gaseous Potassium Release and Ash-Forming
230 Characteristics during Combustion of Biomass. *Energy & Fuels*. 29 (2015) 2555-63.

231 [35] S.D. Stasio, J.L. Legarrec, J.B.A. Mitchell. Synchrotron Radiation Studies of Additives in Combustion, II: Soot
232 Agglomerate Microstructure Change by Alkali and Alkaline-Earth Metal Addition to a Partially Premixed Flame. *Energy*
233 & *Fuels*. 25 (2011) 916-25.

234 [36] X. Wang, S. Li, A. Adeosun, Y. Li, M. Vujanović, H. Tan, et al. Effect of potassium-doping and oxygen concentration
235 on soot oxidation in O₂/CO₂ atmosphere: A kinetics study by thermogravimetric analysis. *Energy Conversion and*
236 *Management*. 149 (2017) 686-97.

237 [37] N.V. Russell, T.J. Beeley, C.K. Man, J.R. Gibbins, J. Williamson. Development of TG measurements of intrinsic char
238 combustion reactivity for industrial and research purposes. *Fuel Processing Technology*. 57 (1998) 113-30.

239 [38] S.L. Niu, C.M. Lu, K.H. Han, J.L. Zhao. Thermogravimetric analysis of combustion characteristics and kinetic
240 parameters of pulverized coals in oxy-fuel atmosphere. *Journal of Thermal Analysis and Calorimetry*. 98 (2009) 267-74.

241 [39] J.P. Neeft, M. Makkee, J.A. Moulijn. Catalysts for the oxidation of soot from diesel exhaust gases. I. An exploratory
242 study. *Applied Catalysis B: Environmental*. 8 (1996) 57-78.

243 [40] A.M. Cunliffe, P.T. Williams. Composition of oils derived from the batch pyrolysis of tyres. *Journal of Analytical and*
244 *applied Pyrolysis*. 44 (1998) 131-52.

245 [41] M. Herrera, G. Matuschek, A. Kettrup. Thermal degradation of thermoplastic polyurethane elastomers (TPU) based on
246 MDI. *Polymer Degradation and Stability*. 78 (2002) 323-31.

247 [42] L. Li, Q. Ren, X. Wang, S. Li, Q. Lu. TG-MS analysis of thermal behavior and gaseous emissions during
248 co-combustion of straw with municipal sewage sludge. *Journal of Thermal Analysis and Calorimetry*. 118 (2014) 449-60.

249 [43] J. Lahaye. Mechanisms of soot formation. *Polymer Degradation and Stability*. 30 (1990) 111-21.

250